AGU ADVANCING EARTH AND SPACE SCIENCES

Earth and Space Science

RESEARCH ARTICLE
10.1029/2023EA002988

Key Points:

- In middle and low thermosphere of below ~300 km, storm-time decreases of the ratio of O/N_2 volume density are mainly caused by O reduction
- In the upper thermosphere, N_2 enhancement plays a vital role in the decreases of the ratio of O/N_2 volume density during the storm
- At all pressure levels, storm-time increases of the ratio of O/N_2 volume density depend more on the N_2 decreases

Supporting Information:

Supporting Information may be found in the online version of this article.

Correspondence to:

Z. Ren,
zpren@mail.iggcas.ac.cn

Citation:

Yu, T., Wang, W., Ren, Z., Cai, X., & He, M. (2023). Vertical variations in thermospheric O/N_2 and the relationship between O and N_2 perturbations during a geomagnetic storm. *Earth and Space Science*, *10*, e2023EA002988. https://doi.org/10.1029/2023EA002988

Received 17 APR 2023
Accepted 10 SEP 2023

Author Contributions:

Conceptualization: Tingting Yu
Funding acquisition: Tingting Yu, Wenbin Wang, Zhipeng Ren
Investigation: Tingting Yu
Methodology: Tingting Yu
Project Administration: Wenbin Wang, Zhipeng Ren
Validation: Tingting Yu, Wenbin Wang
Writing – original draft: Tingting Yu, Maosheng He
Writing – review & editing: Wenbin Wang, Zhipeng Ren, Xuguang Cai

Vertical Variations in Thermospheric O/N_2 and the Relationship Between O and N_2 Perturbations During a Geomagnetic Storm

Tingting Yu[1,2,3,4,5], Wenbin Wang[5], Zhipeng Ren[1,2,3,4], Xuguang Cai[5,6], and Maosheng He[7]

[1]Key Laboratory of Earth and Planetary Physics, Institute of Geology and Geophysics, Chinese Academy of Sciences, Beijing, China, [2]Innovation Academy for Earth Science, Chinese Academy of Sciences, Beijing, China, [3]Beijing National Observatory of Space Environment, Institute of Geology and Geophysics, Chinese Academy of Sciences, Beijing, China, [4]College of Earth and Planetary Sciences, University of the Chinese Academy of Sciences, Beijing, China, [5]High Altitude Observatory, National Center for Atmospheric Research, Boulder, CO, USA, [6]Laboratory of Atmospheric and Space Physics, University of Colorado Boulder, Boulder, CO, USA, [7]Private, Kühlungsborn, Germany

Abstract The ratio of O to N_2 number densities (O/N_2) at different altitudes is an important parameter in describing thermospheric neutral composition changes and their effects on the ionosphere during geomagnetic storms. However, storm-induced vertical variations in O/N_2 and its dependence on the O and N_2 perturbations are still not fully understood. Here, the Thermosphere/Ionosphere Electrodynamics General Circulation Model simulations were used to investigate the responses of thermospheric composition at different pressure levels to the super geomagnetic storm occurred on November 20 and 21 in 2003. Our analysis shows that the behaviors of O/N_2 perturbations on different pressure levels are similar above ~180 km altitude. In the middle and low thermosphere of below ~300 km, the storm-time O/N_2 decrease is mainly caused by a large reduction of O number density. However, N_2 enhancement plays a vital role in O/N_2 decreases in the upper thermosphere. The O/N_2 enhancement is mainly attributed to the N_2 decreases at all pressure levels. The changes of O and N_2 number densities at a constant pressure level can be explained by the perturbations of their mass mixing ratio (mmr) and total mass density (ρ). The regions of the O/N_2 decrease are characterized by the O mmr decrease and N_2 mmr enhancement, whereas the regions of the O/N_2 increase are characterized by the O mmr increase and N_2 mmr decrease. The ρ value that shows the decrease globally at most pressure levels during the storm either enhance or reduce the O and N_2 perturbations.

Plain Language Summary The column O/column N_2 density ratio ($\sum O/N_2$) was usually used to describe thermospheric neutral composition responses to geomagnetic storms and the storm effects on ionospheric plasma density. However, thermospheric circulation changed considerably during the storm, resulting in discrepancies in composition at different altitudes. Additionally, the daytime electron density changes during geomagnetic storms are more related to those of local O/N_2 at a given altitude, not the $\sum O/N_2$. Therefore, it is important to fully understand the storm-induced vertical variations in O, N_2 and O/N_2 perturbations. In this paper, the vertical variations in O/N_2 and its dependence on the O and N_2 perturbations during the 20–21 November 2003 storm are investigated by the numerical simulations. Our results shows that the behaviors of O and N_2 perturbations depend much on the altitude, but those of O/N_2 on different pressure levels are similar, especially above ~180 km. This study helps us better understand the physical process of storm-time $\sum O/N_2$ variations based on the observations.

1. Introduction

The ratios of height-integrated number density of atomic oxygen (O) to that of molecular nitrogen (N_2), namely column O/column N_2 density ratio ($\sum O/N_2$), which can be deduced by disk-viewing optical observations of OI 135.6 nm and Lyman-Birge-Hopfield radiances (Meier, 2021; Strickland et al., 1995), has been widely utilized to describe thermospheric neutral composition responses to geomagnetic storms and the storm effects on ionospheric plasma density (e.g., Cai et al., 2020, 2021a, 2021b, 2023; Crowley et al., 2006; Eastes et al., 2020; Lee et al., 2013; Liou et al., 2005; Strickland et al., 1999, 2001; Wang et al., 2021; Yu et al., 2022a, 2022b; Zhai et al., 2023; Zhang et al., 2004). Previous studies demonstrated the evolution and physical processes of $\sum O/N_2$ during geomagnetic storms, which is briefly summarized as follows. High-latitude Joule heating during a storm induces temperature changes, and causes upward winds and

upwelling of air such that the N_2-rich/O-poor air is bought up from the lower thermosphere (~100 km) into the *F* region (Burns, Killeen, Carignan, & Roble, 1995; Burns, Killeen, Deng et al., 1995; Fuller-Rowell et al., 1994). At the same time, high-latitude temperature enhancement results in a strong equatorward horizontal pressure gradient and enhanced equatorward neutral winds to transmit the N_2-rich/O-poor air to the mid-low latitudes. This seems to imply that the large N_2 increases at high latitudes cause $\sum O/N_2$ depletion, which then extends to mid-low latitudes as the storms proceed (Kil et al., 2013; Meier et al., 2015). On the other hand, downwelling of air occurs at lower latitudes adjacent to the high latitude upwelling region due to thermospheric storm-time circulation changes. This storm-time downwelling of O-rich/N_2-poor air increases $\sum O/N_2$ (Burns, Killeen, Carignan, & Roble, 1995; Burns, Killeen, Deng et al., 1995; Immel et al., 2001; Kil et al., 2013). $\sum O/N_2$ enhancement pattern is also propagated equatorward due to horizontal transport (Cai et al., 2022; Immel et al., 2008).

Other than $\sum O/N_2$, the ratio of O and N_2 number densities at a particular altitude is defined as the ratio of O/N_2 volume density (hereafter simply O/N_2) (Yue et al., 2019). The daytime electron density changes during geomagnetic storms are more related to those of local O/N_2 at a given altitude, not the $\sum O/N_2$ (Crowley & Meier, 2008). This is because electron production is related to the photoionization of local O number density and its loss is proportional to local N_2 number density (Rishbeth, 1998). Burns, Killeen, Carignan, and Roble (1995) and Burns, Killeen, Deng et al. (1995) investigated the storm-time responses of O/N_2 at ~370 km by using the in situ observations of the Dynamics Explorers 2 (DE 2) satellite and the Thermosphere/Ionosphere General Circulation Model. O/N_2 enhancements were observed and simulated during the storm main phase in the middle latitudes in the winter hemisphere. They demonstrated that O/N_2 increases are partially caused by the reduction of N_2 number density. N_2-poor air was brought from higher thermosphere to lower thermosphere. In addition, there was a good correlation between the daytime O/N_2 increases on a constant pressure level and daytime electron density enhancements at the F_2 peak during the storm. Crowley and Meier (2008) also showed that the regions of storm-time O/N_2 increases were consistent with those of electron density enhancements near the *F* layer peak.

These aforementioned previous studies focused on the O/N_2 changes in the *F* region. Based on the Global Ultraviolet Imager (GUVI) limb measurements, Kil et al. (2011a) presented the altitude profiles of the perturbations in O, N_2 and O/N_2 during the 20 November 2003 superstorm at two selected geophysical locations in the height coordinates. The compositional changes in the height coordinates are affected by the thermal contraction and expansion (Burns, Killeen, Carignan, & Roble, 1995; Burns, Killeen, Deng et al., 1995). Kil et al. (2011a) concluded that the storm-time O/N_2 perturbations in the *F* region were mostly determined by the N_2 changes in the height coordinates. Furthermore, they found an inconsistency during the storm between the variations in O/N_2 in the *F* region and those of $\sum O/N_2$. There were only minor changes in O/N_2 in the *F* region where $\sum O/N_2$ increases were observed. Yu et al. (2021a) use the GUVI limb retrievals to investigate the responses of O and N_2 altitude profiles to the 20 November 2003 superstorm. The relative contributions of O and N_2 changes to the O/N_2 responses in the middle thermosphere (~160 km) were presented briefly. They stressed that during the storm main and recovery phases, the middle thermospheric (~160 km) O/N_2 depletion on a constant pressure surface was mostly related to O decreases, whereas O/N_2 enhancement depended primarily on N_2 decreases.

However, GUVI instrument provides approximately 14 orbital data every day corresponding to different UTs/longitudes, thus does not provide global longitude-latitude distribution of neutral composition at a particular UT (Meier et al., 2015). In comparison, numerical simulations can provide storm-time composition perturbations globally for both day and night. Additionally, the previous studies have not fully understood the storm-induced O/N_2 variations at different altitudes and their relationship with O and N_2 perturbations, which are the subjects of this paper. Yu et al. (2021b) employed Thermosphere/Ionosphere Electrodynamics General Circulation Model (TIEGCM) simulations to study O and N_2 responses on a constant pressure surface ($z = -1.5$, ~160 km) during the 20 November 2003 superstorm. Yu et al. (2021b) demonstrated that TIEGCM simulations qualitatively reproduced the GUVI observations. The model captures the large-scale structures of the composition changes during this superstorm, and its temporal evolution of the effects are coincident with the observations. Thus, the model is valuable to investigate the composition perturbations during this storm and can be used to gain insights into the possible physical mechanisms driving these changes. In this paper, based on the general consistency between GUVI measurements and TIEGCM results, we used TIEGCM simulations to further investigate the vertical variations of O/N_2 and their relationship with O, N_2 changes on a global scale during the 20 and 21 November 2003 (day of year (DOY) 324 and 325) superstorm.

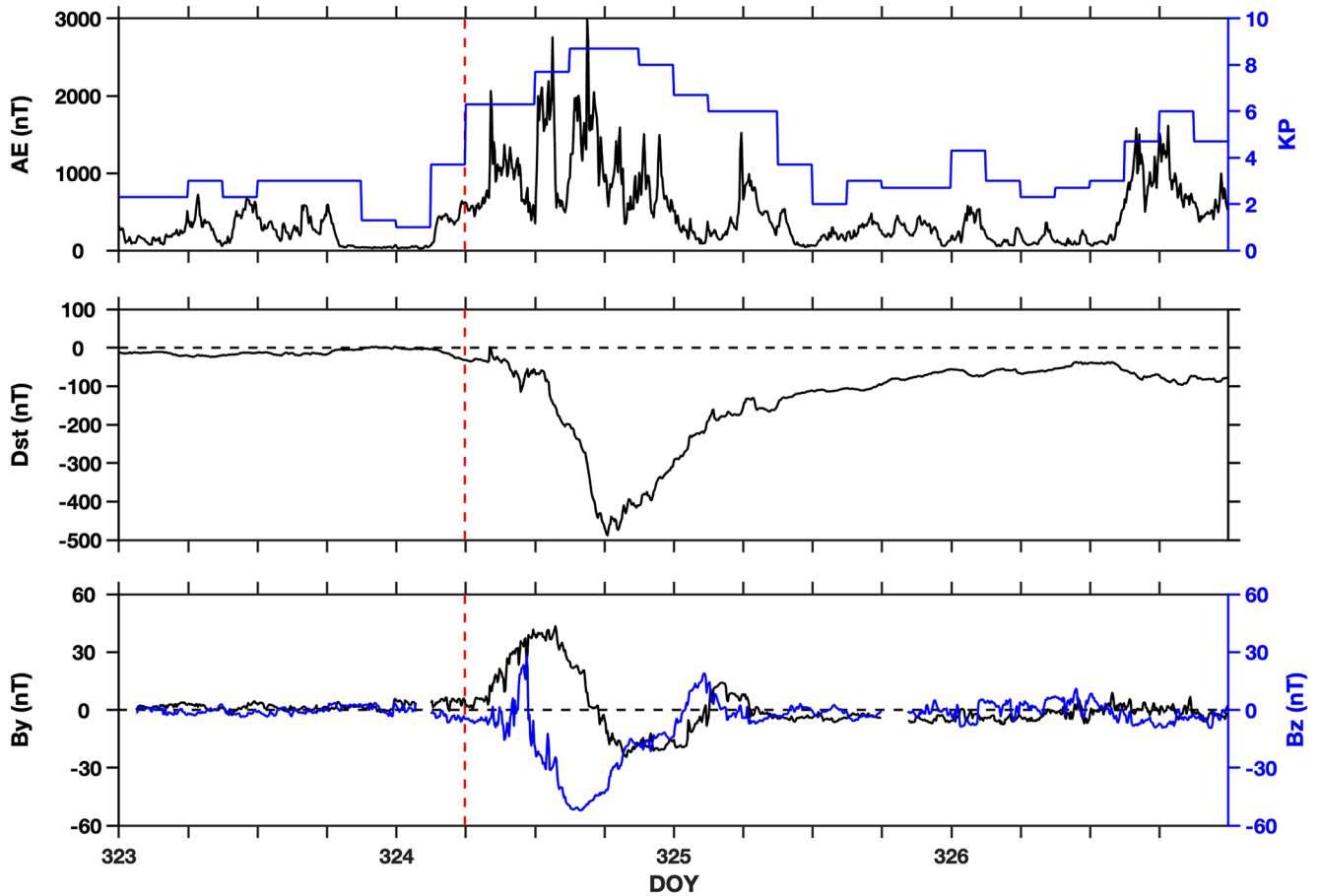

Figure 1. The top panel is the variations of AE (black line) and 3-hr Kp (blue line) indices on day of year 323–326 in 2003; the second panel is the hourly Dst index, and the black dashed line is the zero value of the Dst index; the third panel is the y (By, black line) and z (Bz, blue line) component of the interplanetary magnetic field. The black dashed line is the zero value of By and Bz. The red dashed line indicates the storm onset time.

2. TIEGCM Simulation

The TIEGCM is a three-dimensional, time-dependent, global thermosphere-ionosphere model that can self-consistently simulate composition, dynamics, circulation, electrodynamics, photoionization and chemistry in the thermosphere from ∼97 to 600 km (Richmond et al., 1992; Roble et al., 1988). The TIEGCM utilized a spherical coordinate system with longitude and latitude as the horizontal coordinates and pressure surfaces as the vertical coordinate. The version used here has a high horizontal resolution of 1.25° × 1.25° in geographic longitude and latitude, and a vertical resolution of 0.25 scale height. Solar EUV irradiance input and auroral electron precipitation input of the model are based on Solomon and Qian (2005) and Roble and Ridley (1987), respectively. The Heelis empirical model (Heelis et al., 1982) is used as the high-latitude input. The monthly tidal climatology (Hagan & Forbes, 2002, 2003) is used as the lower boundary input.

3. Results and Discussion

3.1. Geophysical Conditions

The variations of the geomagnetic activity indices from DOY 323 to 326 in 2003 are shown in Figure 1. On DOY 323, 3-hr Kp (blue line) index was less than 3, and AE (black line) index was less than ∼500 nT (the top panel). The absolute values of the hourly Dst index (the second panel), and interplanetary magnetic field (IMF) By and Bz components (the third panel) were close to zero. Thus, DOY 323 was chosen as the quiet-time reference. Kp and AE indices started to increase sharply at ∼6 UT on DOY 324 (red dashed line), and both the By and Bz components also began to change rapidly. This means the storm onset. The Kp and AE indices reached maxima

of 9- and ~3,000 nT at ~15 UT on DOY 324, and then decreased to the minima of 2 and ~100 nT at ~12 UT on DOY 325, respectively. During this period (~6 UT on DOY 324 to ~12 UT on DOY 325), Dst index decreased slowly from ~6 UT to ~12 UT on DOY 324. It then rapidly decreased from ~12 UT to reach a minimum of ~−490 nT at ~18–20 UT on DOY 324, and then began to recover. The IMF By component had negative values from ~17 UT on DOY 324 to ~3 UT on DOY 325, and was positive for the rest of the period. Bz remained southward (negative) for a long period of time, except for a few hours of northward at about 10–11 UT on DOY 324 and at ~1–5 UT on DOY 325. IMF By and Bz had large magnitudes of around 50 nT during the storm period. The magnitudes of these parameters became small from ~12 UT on DOY 325 until ~14 UT on DOY 326. According to the variations of the geomagnetic indices, the initial phase of the storm was from ~6 UT to ~12 UT on DOY 324. The storm main phase was approximately from ~12 UT to ~20 UT on DOY 324. The storm recovery phase began after that.

3.2. Composition Variations on the $z = -1.5$ Pressure Surface (~160 km)

Before the discussion of composition perturbations in vertical direction, we first present the modeled relative contributions of storm-time O and N_2 changes to the O/N_2 responses in the middle thermosphere ($z = -1.5$ pressure surface at ~160 km in the TIEGCM simulation). We selected three UTs from the storm initial (14.38 UT on DOY 324), main (19.24 UT on DOY 324) and recovery (6.29 UT on DOY 325) phases to show the latitude and local time distribution of the storm-induced percentage changes ((storm-quiet)/quiet) in O/N_2, O and N_2 number densities in Figure 2 (first -third rows). In addition, we calculated the differences of the absolute values of O and N_2 percentage changes to present their relative magnitudes in O/N_2 perturbations (the fourth row).

Figure 2 shows that in the pressure coordinate, the storm-time O can be either increased or decreased with different magnitudes in different longitude and latitude regions over the entire storm period. Whereas N_2 decreased almost in all regions on this pressure level over the entire storm period, except in some regions at high latitudes where N_2 had an enhancement. Comparing the changes between O, N_2 and O/N_2 in the regions of O/N_2 decreases shown in Figure 2 and in the pressure coordinates, we can see that during the initial phase of the storm, O decreased by ~30–60%. N_2 increased by about 20%–50% at high latitudes in the Northern Hemisphere (NH), but decreased in other regions by ~20%. During the main and recovery phases of the storm and in regions of O/N_2 decreases, O decreased by more than 100%, and N_2 deceased at most regions by ~5–40%. The differences between the absolute values of O and N_2 percentage changes in the fourth row are mostly greater than zero (0–~80%), which indicates that O had larger changes (reduction) relative to N_2 in the regions of O/N_2 depletion, though their changes depended on the longitude and latitude. Thus, O/N_2 decreases during the storm were primarily caused by a large O reduction on this constant pressure surface. It is worth noting that O/N_2 decreases in the summer Southern Hemisphere (SH) had an extended latitudinal range relative to those in the winter NH. The hemispheric asymmetry is partly due to the summer-to-winter prevailing circulation, meanwhile, there existed the more intensive Joule heating and ion drag in the summer SH, resulting in the stronger temperature gradients and equatorial wind perturbations in the SH (Fuller-Rowell et al., 1994; Yu et al., 2021a).

In the regions of O/N_2 enhancement, the composition responses during this superstorm are a bit more complicated. During the initial phase of the storm, N_2 decreased by ~10–20%, but O changes were close to zero except in two regions (~0°–~45° S, ~14–~18.5 LT; ~40°–~60° S, ~18–~21.5 LT) where O increased by ~30%. During the main and recovery phases, N_2 decreased by ~40–80% in the regions of O/N_2 increases. O was increased or decreased, but the magnitude was less than 20%. The differences between the absolute values of O and N_2 percentage changes were mostly negative (0–40%), which indicates a larger contribution of N_2 number density changes to O/N_2 increases in most regions. Therefore, the storm-induced O/N_2 enhancement in the middle thermosphere is primarily attributed to the large decreases of N_2.

However, a larger O increase (~50%) was seen in the ~0°–~45° S latitudes near ~12–~17 LT in the SH during the storm initial phase. The differences between the absolute values of O and N_2 percentage changes were greater than zero, indicating the important effects of O to O/N_2 increases. Yu et al. (2021b) demonstrated that this O increase was due to the day-to-day variation of the thermosphere, mainly caused by the horizontal advection. Additionally, there was another larger O increase (~40%) occurred in the ~40°–~60° S latitude range near ~18–~21 LT in the storm initial phase. The two large O increases gradually merged and were transported to the ~0–~45° S latitude range near ~23–~2 LT in the storm main phase. The differences between the absolute values of O and N_2 percentage changes were near zero during the main phase in the region, which indicates that the

10.1029/2023EA002988

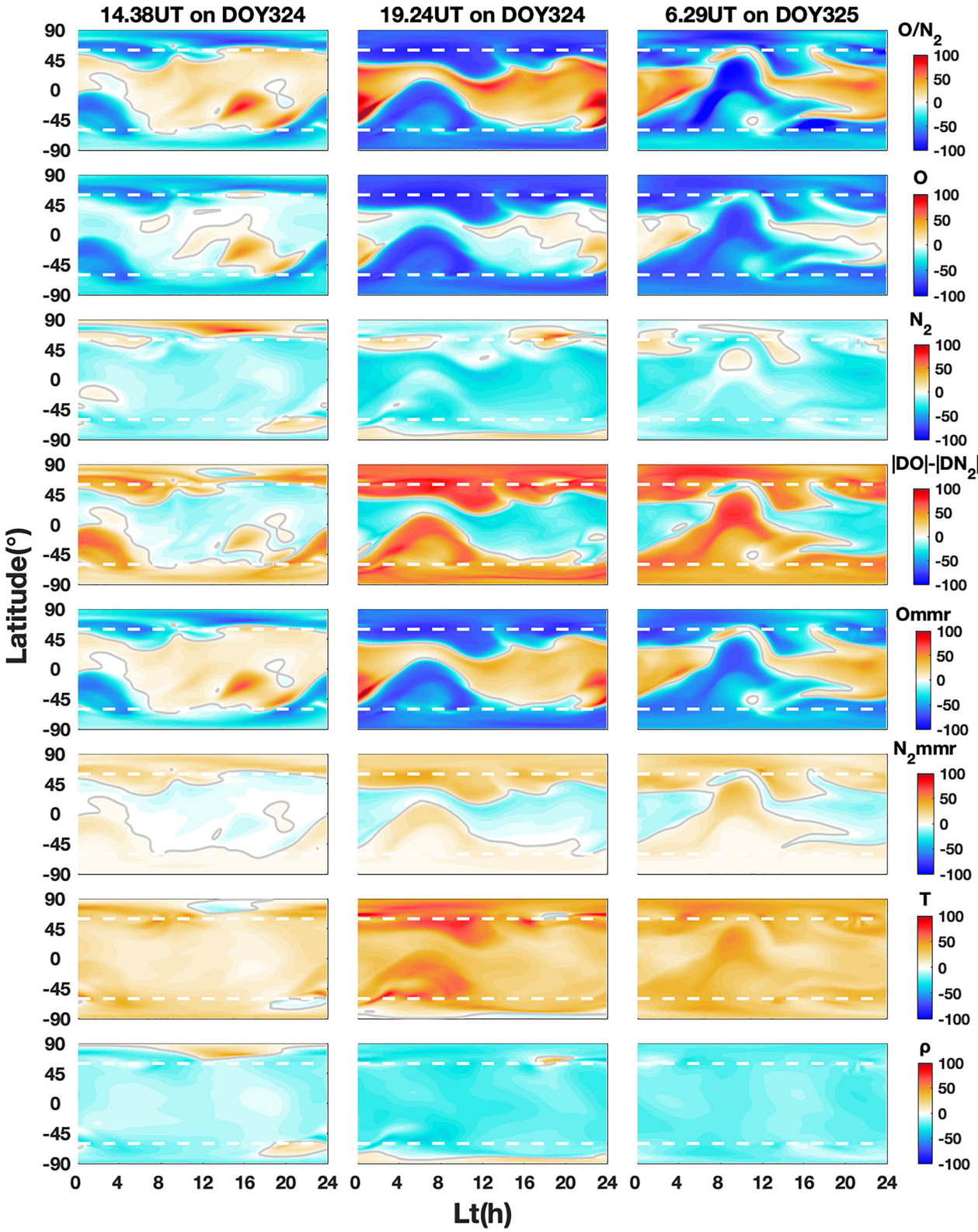

Figure 2. (top to bottom) Latitude and local time distributions of the percentage changes ((storm-quiet)/quiet) of O/N_2, O, and N_2 number densities, the differences of absolute value of O and N_2 percentage changes, O mass mixing ratios (O mmr) and N_2 mass mixing ratios (N_2 mmr), temperature (T) and total mass density (ρ) on the $z = -1.5$ (~160 km) pressure surface at three UTs (left to right). In each panel the gray curves indicate the zero value, and the two white dashed lines are the latitude of ±60°.

O and N_2 changes are both important in determining the storm-time O/N_2 enhancement in this region. This O increase resulted from the downwelling at high latitudes and then were propagate to middle-low latitudes by the horizontal advection, referring to Movie S2 in Yu et al. (2021b). Therefore, the storm-induced O/N_2 enhancement in the middle thermosphere was dependent more on the large N_2 decreases, except in some regions where O/N_2 enhancement was dominated both by O and N_2 changes.

Next, we investigate the causes of the behaviors of O and N_2 number densities in the middle thermosphere through TIEGCM simulations. TIEGCM calculates the mass mixing ratio (mmr) of O and N_2 (O mmr, Ψ_o and N_2 mmr, Ψ_{N_2}), and their relationship with the total air mass density can be described as the following:

$$\Psi_o = \rho_o/\rho \,(\text{where } \rho_o = m_o n_o)$$

$$\Psi_{N_2} = \rho_{N_2}/\rho \left(\text{where } \rho_{n_2} = m_{N_2} n_{N_2}\right) \tag{1}$$

where ρ_0 is the O mass density with atomic mass m_o, and n_o is the O number density. ρ_{N_2} is the N_2 mass density with molecular mass m_{N_2}, and n_{N_2} is the N_2 number density. ρ is the total mass density. Therefore, the differential changes of O (N_2) number density can be expressed as:

$$d\rho_o/\rho_o = dn_o/n_o = d\Psi_o/\Psi_o + d\rho/\rho$$

$$d\rho_{N_2}/\rho_{N_2} = dn_{N_2}/n_{N_2} = d\Psi_{N_2}/\Psi_{N_2} + d\rho/\rho \tag{2}$$

where d is the differential sign. The storm-quiet percentage changes ((storm-quiet)/quiet) of O (N_2) number density can refer to Equation 2 to assess the contribution from their mass mixing ratios and the total mass density. Note that the differential equation is mainly valid for small changes, thus cannot be used to quantitatively estimate the storm-quiet changes. However, it is appropriate to evaluate their respective signs in Equation 2.

The ideal gas law:

$$P = \rho RT \tag{3}$$

P is the pressure, R is gas constant, and T is the neutral temperature. Thus, in pressure coordinates, as the temperature increases (decreases) during the storm, ρ must decrease (increase) to maintain a constant pressure on a particular pressure surface.

The latitude and local time distribution of storm-quiet percentage differences of O mmr, N_2 mmr neutral temperature (T) and total mass density (ρ) at the same UTs are included in Figure 2 (fifth -eighth rows). Furthermore, a movie of the parameters in Figure 2 (Movie S1) is provided in the Supporting Information (SI) to illustrate in detail the temporal and spatial evolution of composition responses on DOY 324 and 325.

Since $\Psi_o + \Psi_{N_2} \cong 1$ at ~160 km, the increases of Ψ_o are approximately equivalent to the decreases of Ψ_{N_2} (Burns et al., 1989). N_2 is the major gas species on the $z = -1.5$ pressure surface, thus, Ψ_{N_2} is larger relative to Ψ_o, leading to the smaller percentage changes of Ψ_{N_2} than those of Ψ_o globally shown in Figure 2. Comparing the changes of O/N_2 with those of O mmr and N_2 mmr, in the regions of O/N_2 depletion, O mmr decreased and N_2 mmr increased, which were determined mainly by the upwelling of high Ψ_{N_2} (low Ψ_o) air from the low thermosphere at high latitudes and the horizontal advection to mid-low latitudes (Burns et al., 2006). In the regions of O/N_2 increases, the O mmr had an enhancement and N_2 mmr had a decrease, which were dependent more on the downwelling of the high Ψ_o (low Ψ_{N_2}) air in the upper thermosphere at high latitudes and horizontal transport. ρ (last row) decreased in almost all regions on this pressure level (−1.5, ~160 km) over the entire course of the storm, except at high latitudes on DOY 324 where it slightly increased. The ideal gas law (Equation 3) shows that ρ decreases in almost all regions were mainly due to the increases of neutral temperature shown in Figure 2. According to Equation 2, ρ reduction plus the decreases of O mmr and N_2 mmr can generate large decreases of O and N_2 number densities. By comparison, ρ reduction plus the increases of O mmr and N_2 mmr can cause small increases or even decreases of O and N_2 number densities. Therefore, in all regions of N_2 mmr enhancement on this pressure level, the N_2 mmr enhancement (0–~40%) with the ρ reduction (0–45%) resulted in the decreases of N_2 number density in these regions. At high latitudes of NH at 14.38 UT on DOY 324, the increases of N_2 number density with a maximum of ~80% were caused by the enhancement of N_2 and ρ. In all regions of N_2 mmr decreases at mid-low latitudes, N_2 mmr decreases (0–~20%) with ρ reduction (0–40%) resulted in the larger

10.1029/2023EA002988

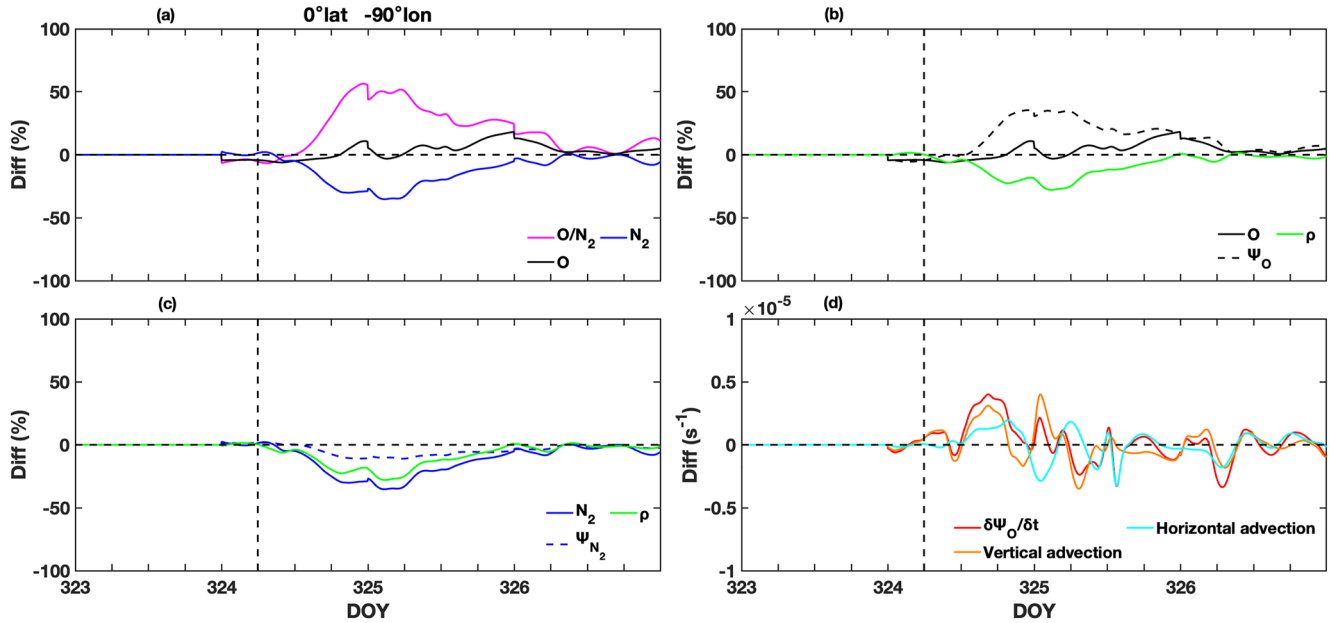

Figure 3. (a) Variations of the percentage changes in O/N_2, O, and N_2 number densities as a function of time at the location of 0°N, 90°W; (b) variations of O number density, atomic oxygen mass mixing ratios (Ψ_o) and total mass density (ρ); (c) variations of N_2 number density, molecular nitrogen mass mixing ratios (Ψ_{N_2}) and total mass density (ρ); (d) Variations of the storm-quiet changes in the total time rate of change of O ($\partial\Psi_o/\partial t$), horizontal advection and vertical advection of O.

decreases of N_2 number density in these regions. Thus, N_2 number density decreased almost globally on this pressure level. Similarly, the O mmr enhancement at mid-low latitudes was also weakened by the ρ reduction, which showed small changes of O number density except in the two regions with O increases of ~40% and ~30% during the initial and main phases of the storm. In addition, the decreases of O mmr, in conjunction with the ρ reduction, led to larger decreases of O number density on this pressure level, with a maximum magnitude of ~70% at 14.38 UT on DOY 324, ~85% at 19.24 UT on DOY 324, and ~80% at 6.29 UT on DOY 325.

To show clearly the behavior and cause of storm-time composition changes, we selected two locations (0°, 90°W; 40°S, 75°E) to show the variations of composition and diagnostic terms (cf. Burns et al., 2006) as a function of time on the $z = -1.5$ (~160 km) pressure surface. Figure 3a shows the percentage differences of O/N_2 (pink line), O (black line) and N_2 (blue line) number densities from DOY 323 to 326 at the equator (0°, 90°W). Storm-time O/N_2 was larger than the quiet-time value for most of the times during the storm at this location; O was slightly decreased before 18 UT on DOY 324, but slightly increased after that; while N_2 had a large decrease during the entire storm period. Therefore, the storm-time O/N_2 enhancement on this pressure level at this location depend mainly on the N_2 decreases. The causes of O changes are shown in Figure 3b: the storm-time increases of Ψ_o (black dashed line) were offset by the decreases of ρ (green line). Figure 3c shows that Ψ_{N_2} had a small decrease on this pressure level. The tendency of N_2 percentage changes was basically the same as that of ρ changes. Figure 3d shows the changes in the total time rate of change of O ($\partial\Psi_o/\partial t$), and horizontal and vertical advection of O. The comparison of the morphology and magnitude between the horizontal (cyan line) and vertical (yellow line) advection with $\partial\Psi_o/\partial t$ (red line) shows that both the vertical and horizontal advection were crucial to the change of Ψ_o at this location.

Figure 4 is the same format as Figure 3, but at the location of 40°S, 75°E. Figure 4d shows that the storm-time responses at this location were mainly driven by the horizontal advection. The O/N_2 increase at 0 UT on DOY 324 was the day-to-day variation mentioned before. The second O/N_2 increase occurred from ~12 UT to 18 UT on DOY 324. Obviously, this O/N_2 increase was the result of the downwelling at high latitudes and then propagated to this location by the horizontal advection (See Movie S1). Movie S1 shows that the O/N_2 increase near this location changed to large decreases along as the storm progressed. Figure 4a shows that O and N_2 both played a role in this O/N_2 enhancement. O/N_2 storm-time decreases, such as that occurred from ~18 UT on DOY 324 to 12 UT on DOY 325 (Figure 4a), were primarily caused by the large O reduction. Figure 4b shows that the O changes depended more on the Ψ_o changes compared to those of ρ. Ψ_{N_2} changed a little on this pressure level, and the tendency of N_2 changes was almost the same as that of ρ changes (Figure 4c).

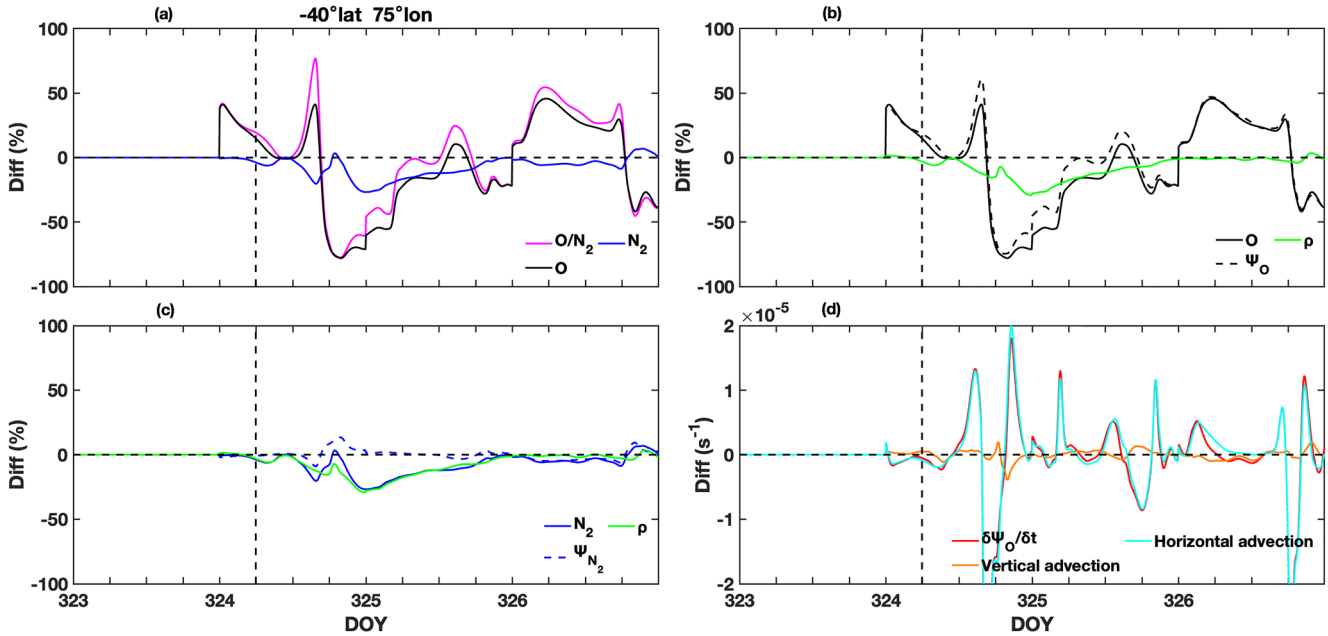

Figure 4. Same as Figure 3, but at the location of 40°S, 75°E.

Furthermore, Figure S1 in Supporting Information S1 shows the total time rate of change of N_2 ($\partial\Psi_{N_2}/\partial t$), and horizontal and vertical advection of N_2. Similar to O, horizontal advection and vertical advection dominated the storm-induced N_2 changes at the location of 0°, 90°W. At the location of 40°S, 75°E, storm-time N_2 responses were mainly driven by the horizontal advection. Thus, the changes of O and N_2 number densities can be explained by the changes of their mass mixing ratio and ρ. The storm-induced changes of Ψ_o and Ψ_{N_2} depend primarily on the upwelling and downwelling of air and horizontal advection. The global ρ reduction during the storm is due to the storm-induced temperature enhancement.

3.3. Changes in the Vertical Direction

Figure 5 shows the pressure surface-latitude distributions of storm-quiet percentage changes in O/N_2, O, N_2 number density and the differences of absolute value of O and N_2 changes, and the percentage changes of O mmr, N_2 mmr, neutral temperature and total mass density at the longitude of 0° at the same UTs as in Figure 2. The vertical axis is in pressure coordinates from $z = -4$ (~120 km) to $z = 4$ (~450 km). Table in the SI show the different pressure levels and their corresponding approximate altitudes. Additionally, Figure S2 in Supporting Information S1 shows the changes of these parameters in altitude coordinate for the quantitative presentation of the effects from the thermal expansion. Movie S2 shows the temporal evolution of the parameters in Figure 5 on DOY 324 and 325. Figure 5 indicates that the behaviors of O/N_2 perturbations on different pressure levels were similar above the $z = \sim -1.5$ (~180 km) pressure level. As is mentioned in the Introduction, the storm-time electron density changes are more relevant to the local O/N_2 changes at a given altitude, not the $\sum O/N_2$. However, the correlation between the peak electron density in the F layer and $\sum O/N_2$ have been investigated by many studies based on the thermospheric and ionospheric observations (Kil et al., 2011b; Lee et al., 2013; Strickland et al., 2001). O and N_2 column densities in the middle thermosphere (~140–180 km) make a major contribution to $\sum O/N_2$, due to the exponential decay of O and N_2 number densities with altitude (Strickland et al., 1995; Yu et al., 2020, 2021a; Yue et al., 2019). Therefore, the storm-induced electron density variations in the ionosphere F_2 region are sometimes closely correlated with the neutral composition perturbation in the middle thermosphere, which can be explained by the similar perturbation morphology of O/N_2 at different altitudes as shown in Figure 5. Similarly, Lei et al. (2010) emphasized the high correlation between O/N_2 on the $z = 3$ (~400 km) pressure surface and $\sum O/N_2$. In the middle and low thermosphere below ~180 km, the O/N_2 perturbations were highly dependent on the altitude, and related to the storm evolution. The storm-induced perturbations of O and N_2 number densities had significant latitude dependence at all pressure levels, which were also changing as the storm progressed.

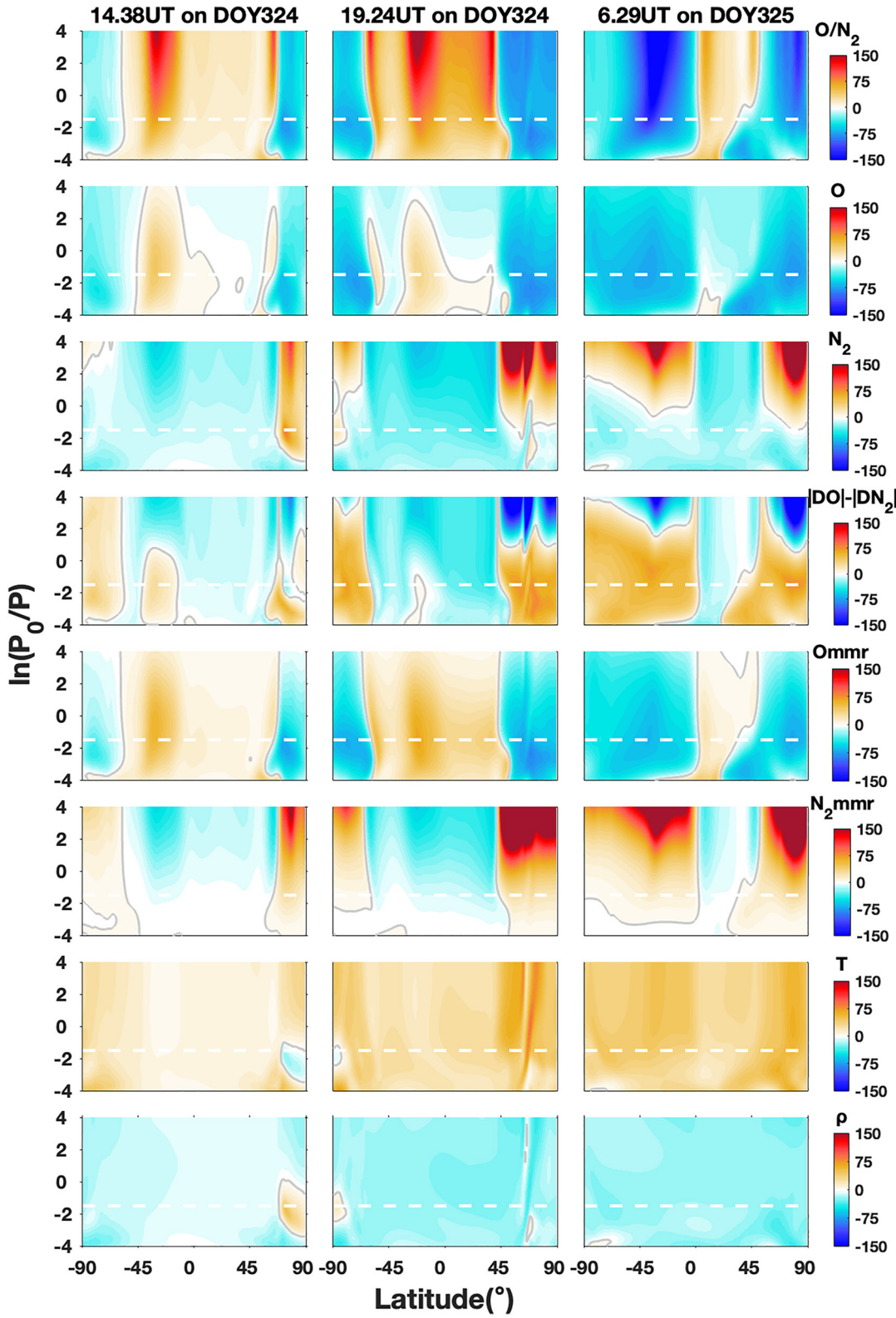

Figure 5. (top to bottom) The percentage changes in O/N_2, O, N_2 number density, the differences of absolute value of O and N_2 percentage changes, O mass mixing ratios (O mmr), N_2 mass mixing ratios (N_2 mmr), temperature (T) and total mass density (ρ) in pressure coordinates at the longitude of 0° at three UTs (left to right). In each panel the gray curves indicate the zero value, and the white dashed line is the $z = -1.5$ pressure surface.

We first analyze the storm-time perturbation behaviors of O mmr and N_2 mmr shown in Figure 5. In the storm initial phase (14.38 UT), weak upwelling at high latitudes occurs as a result of the increased temperature, and high Ψ_{N_2} (low Ψ_o) air in the low thermosphere was transported to the upper thermosphere. Thus, a small reduction of O mmr (0–∼70%) and an enhancement of N_2 mmr (0–∼180%) occurred at all pressure levels of the high latitudes. At the same time, the downwelling at lower latitudes leads to the opposite perturbation behaviors of O mmr (increase of 0–∼60%) and N_2 mmr (decrease of 0–∼60%). The temperature differences in the latitudinal direction were also set up, leading to an equatorward pressure gradient, which drove equatorward horizontal winds. The equatorward flow carried the composition changes to lower latitudes. As the storm proceeded, in the storm main phase (19.24 UT), upward and downward winds both became much stronger, which resulted in considerably larger composition changes. The temperature differences in the latitudinal direction were also large, resulting in a strong equatorward flow. Thus, the reduction of O mmr (0–∼85%) and the increases of N_2 mmr (0–∼850%) at high latitudes were transported to a wider latitude range during the main phase of the storm, which is the result of horizontal transport effects (Burns et al., 2006). The latitudinal and altitudinal dependency of composition perturbations is partly determined by the magnitude differences of horizontal wind perturbations at different altitudes and latitudes during the storm. During the recovery phase of the storm (6.29 UT on DOY 325), O mmr reduction of 0–∼65% (N_2 mmr enhancement of 0–∼550%) in the SH was transported to the equator. While the O mmr reduction (0–∼70%) and N_2 mmr enhancement (0–∼750%) extended to ∼45° N above the $z = \sim -1$ pressure level in the NH, and the lowest latitude of O mmr reduction changed gradually to ∼20° N at $z = -4$ pressure level at this longitude. Additionally, the O mmr changes (increase and decrease) had a maximum along with the altitude over the entire storm period, mainly on the $z = -1.5$ pressure surface. However, N_2 mmr changes increased with the increase of altitude.

Figure 5 shows that the total mass density (last row) decreased almost at all pressure levels except in some regions at the high latitudes of NH at 14.38 UT where it had an increase. This should be also explained by the temperature variations in pressure coordinates. Thus, the decreased total mass density, in conjunction with the changes of O mmr and N_2 mmr, explained the perturbation behaviors of O and N_2 number densities. In the storm initial phase (14.38 UT), small N_2 mmr increases (<∼30%) at the high latitudes of the SH plus the ρ reduction (0–∼50%) resulted in the decreases of N_2 number density in these regions. At high latitudes of the NH, however, N_2 increased with a maximal magnitude of ∼75%. During the main and recovery phases of the storm, N_2 decreased at mid-high latitudes in the middle thermosphere due to the offset between the ρ reduction and the small N_2 mmr increases. Whereas at mid-high latitudes in the middle and upper thermosphere (above $z = \sim -1$ pressure level), N_2 has an enhancement, and the enhancement increased with altitude, reaching more than 700% at mid-high pressure levels. Similarly, ρ reduction can offset the enhancement of O mmr at mid-low latitudes. Thus, the O number density had a small enhancement (0∼30%) or even a small decrease of less than ∼20% in the region of O mmr enhancement during the entire storm. ρ reduction contributes to the decreases of O mmr at mid-high latitudes and N_2 mmr at mid-low latitudes at all pressure levels. Therefore, in these regions of O mmr and N_2 mmr decreases, O number density had a decrease of 0–∼85%, and N_2 number density had a decrease of 0–∼45% during the storm. The global decreases of N_2 number density were observed in the middle thermosphere, which were deviated from the previous cognition about the storm-time N_2 increases at high latitudes in altitudes coordinates.

Now we analyze the relative contributions of the storm-time perturbations of O, N_2 number density to O/N_2 variations. The fourth row shows the main reasons of O/N_2 perturbations at different latitudes and pressure levels. In the regions of O/N_2 enhancement (cf. first row, Figure 5), mostly at middle and low latitudes, the negative values of the absolute difference of O and N_2 percentage changes (0– ∼ –50%) indicate that the percentage changes of O (decrease or increase) are smaller than those of N_2. Thus, O/N_2 enhancement at middle and low latitudes was more related to the N_2 decrease at all pressure surfaces during the entire storm period. It should be noted that there is a special region in the initial and main phases of the storm, where the absolute difference of O and N_2 percentage changes is positive (0–∼25%). At 14.38 UT on DOY 324, the region was located at ∼45° S–10° S between $z = \sim -4 - \sim 1$ pressure levels, and it shrunk to ∼30° S–∼10° S latitude range from $z = \sim -4$ to -1 pressure levels at 19.24 UT on DOY 324. The positive values indicate the important effects of O to O/N_2 increases in this region. As aforementioned in Section 3.2, the composition perturbations in this region were mainly driven by the horizontal advection, corresponding to the large O increases in the ∼0°–∼45° S latitudes at 14.38 UT and 19.24 UT on DOY 324 in Figure 2. Movie S2 shows the evolution of the responses more clearly.

The main cause of O/N_2 decreases depends on altitude. At 14.38 UT on DOY 324, the absolute differences of O and N_2 percentage changes are positive with a magnitude of 0–∼40% at all pressure levels of SH in the regions

of O/N_2 decreases (cf. first row, Figure 5). O decrease plays a vital role in the O/N_2 decreases in these regions. However, negative values of the absolute difference (0- ~ -100%) occurred above $z = \sim 0$ pressure level in the NH in the regions of O/N_2 depletion, which indicates that N_2 enhancement can be significant in the upper thermosphere. At 19.24 UT on DOY 324, at mid-high latitudes, N_2 increases have a larger contribution to O/N_2 decreases above the $z = \sim 3$ pressure level in the SH, while above the $z = \sim 1$ pressure level (~300 km) in the NH. Therefore, there exist transition heights of the contributions from O and N_2 number densities to O/N_2 decreases during the storm. Above the transition heights, the storm-time O/N_2 depletion is more related to the large N_2 enhancement. At 6.29 UT on DOY 325, O/N_2 decreases in the SH were transported to the equator. The transition heights were at $z = 1.5$ pressure level at ~30° S, and increased to both sides in the latitude range of O/N_2 depletion in the SH. In the NH, O/N_2 decreases extended to ~45° N above the $z = \sim -1$ pressure level. The transition heights were at about $z = 0.5$ pressure level at ~80° N, and also increased to both sides in the latitude range of O/N_2 depletion in the NH. Therefore, the contributions from O and N_2 number densities to O/N_2 decreases on different pressure levels have altitude and latitude differences. Storm-induced O/N_2 depletion is more related to the O reduction at lower thermosphere (below the transition heights), but depend on the N_2 enhancement in the upper thermosphere (above the transition heights).

4. Conclusion

A first principles model of the coupled thermosphere and ionosphere (TIEGCM) was used to investigate the vertical variations of thermospheric O/N_2 at different pressure levels and its dependence on the O and N_2 perturbations during the November 20 and 21, 2003 superstorm event. The main conclusions are:

1. In the middle and low thermosphere of below ~300 km, the storm-time O/N_2 depletion is primarily associated with a large reduction of O number density. In the upper thermosphere of above ~300 km, N_2 enhancement plays an important role in the O/N_2 decreases.
2. The contributions of O and N_2 perturbations to O/N_2 enhancement are similar at all pressure levels. The storm-induced O/N_2 enhancement was mainly related to the large N_2 decreases, except in some regions where O and N_2 changes are both important for O/N_2 changes.
3. In the regions of O/N_2 decreases, O mmr decreased and N_2 mmr increased at all pressure levels, driven by the upwelling of high Ψ_{N_2} (low Ψ_o) air from the lower thermosphere and horizontal advection. In the regions of O/N_2 increases, O mmr enhanced and N_2 mmr decreased, driven by both the downwelling of low Ψ_{N_2} (high Ψ_o) air from the upper thermosphere and horizontal transport.
4. The total mass density at constant pressure levels decreased almost globally over the entire storm period due to temperature increases. The storm-induced perturbations of O and N_2 number densities can be explained by the superposition of changes of their mass mixing ratio and total mass density.

Data Availability Statement

AE, Dst, Kp, B_y and B_z indices are from https://cdaweb.gsfc.nasa.gov/cdaweb/sp_phys/. The TIEGCM simulation results are available at https://doi.org/10.5281/zenodo.7479451 (Yu, 2022).

Acknowledgments
We thank the support from the B-type Strategic Priority Program of the Chinese Academy of Sciences (XDB41000000), National Key R & D Program of China (Grant 2022YFF0503901), National Science Foundation of China (41874179, 42104009, 42304178), Open Research Project of Large Research Infrastructures—"Study on the interaction between low/mid-latitude atmosphere and ionosphere based on the Chinese Meridian Project," Key Research Program of the Chinese Academy of Sciences (ZDRE-KT-2021-3), fellowship of China Postdoctoral Science Foundation (2021M703192). NCAR is sponsored by the National Science Foundation.

References

Burns, A. G., Killeen, T. L., Carignan, G. R., & Roble, R. G. (1995). Large enhancements in the O/N_2 ratio in the evening sector of the winter hemisphere during geomagnetic storms. *Journal of Geophysical Research*, *100*(A8), 14661–14671. https://doi.org/10.1029/94ja03235

Burns, A. G., Killeen, T. L., Deng, W., Carignan, G. R., & Roble, R. G. (1995). Geomagnetic storm effects in the low-to middle-latitude upper thermosphere. *Journal of Geophysical Research*, *100*(A8), 14673–14691. https://doi.org/10.1029/94ja03232

Burns, A. G., Killeen, T. L., & Roble, R. G. (1989). Processes responsible for the compositional structure of the thermosphere. *Journal of Geophysical Research*, *94*(A4), 3670–3686. https://doi.org/10.1029/ja094ia04p03670

Burns, A. G., Wang, W., Killeen, T. L., Solomon, S. C., & Wiltberger, M. (2006). Vertical variations in the N_2 mass mixing ratio during a thermospheric storm that have been simulated using a coupled magnetosphere-ionosphere-thermosphere model. *Journal of Geophysical Research*, *111*(A11), A11309. https://doi.org/10.1029/2006JA011746

Cai, X., Burns, A. G., Wang, W., Qian, L., Pedatella, N., Coster, A., et al. (2021a). Variations in thermosphere composition and ionosphere total electron content under "geomagnetically quiet" conditions at solar-minimum. *Geophysical Research Letters*, *48*(11), e2021GL093300. https://doi.org/10.1029/2021GL093300

Cai, X., Burns, A. G., Wang, W., Qian, L., Solomon, S. C., Eastes, R. W., et al. (2020). The two-dimensional evolution of thermospheric $\Sigma O/N_2$ response to weak geomagnetic activity during solar-minimum observed by GOLD. *Geophysical Research Letters*, *47*(18), e2020GL088838. https://doi.org/10.1029/2020GL088838

Cai, X., Burns, A. G., Wang, W., Qian, L., Solomon, S. C., Eastes, R. W., et al. (2021b). Investigation of a neutral "tongue" observed by GOLD during the geomagnetic storm on May 11, 2019. *Journal of Geophysical Research: Space Physics*, *126*(6), e2020JA028817. https://doi.org/10.1029/2020JA028817

Cai, X., Wang, W., Burns, A., Qian, L., & Eastes, R. W. (2022). The effects of IMF B_y on the middle thermosphere during a geomagnetically "quiet" period at solar minimum. *Journal of Geophysical Research: Space Physics*, *127*(5), e2021JA029816. https://doi.org/10.1029/2021ja029816

Cai, X., Wang, W., Lin, D., Eastes, R. W., Qian, L., Zhu, Q., et al. (2023). Investigation of the Southern Hemisphere mid-high latitude thermospheric $\sum O/N_2$ responses to the Space-X storm. *Journal of Geophysical Research: Space Physics*, *128*(3), e2022JA031002. https://doi.org/10.1029/2022JA031002

Crowley, G., Hackert, C. L., Meier, R. R., Strickland, D. J., Paxton, L. J., Pi, X., et al. (2006). Global thermosphere-ionosphere response to onset of 20 November 2003 magnetic storm. *Journal of Geophysical Research*, *111*(A10), A10S18. https://doi.org/10.1029/2005JA011518

Crowley, G., & Meier, R. R. (2008). Disturbed O/N_2 ratios and their transport to middle and low latitudes. *Geophysical Monograph Series*, 221–234. https://doi.org/10.1029/181gm20

Eastes, R. W., McClintock, W. E., Burns, A. G., Anderson, D. N., Andersson, L., Aryal, S., et al. (2020). Initial observations by the GOLD mission. *Journal of Geophysical Research: Space Physics*, *125*(7), e2020JA027823. https://doi.org/10.1029/2020ja027823

Fuller-Rowell, T. J., Codrescu, M. V., Moffett, R. J., & Quegan, S. (1994). Response of the thermosphere and ionosphere to geomagnetic storms. *Journal of Geophysical Research*, *99*(A3), 3893–3914. https://doi.org/10.1029/93ja02015

Hagan, M. E., & Forbes, J. M. (2002). Migrating and nonmigrating diurnal tides in the middle and upper atmosphere excited by tropospheric latent heat release. *Journal of Geophysical Research*, *107*(D24), 4754. https://doi.org/10.1029/2001JD001236

Hagan, M. E., & Forbes, J. M. (2003). Migrating and nonmigrating semidiurnal tides in the upper atmosphere excited by tropospheric latent heat release. *Journal of Geophysical Research*, *108*(A2), 1062. https://doi.org/10.1029/2002JA009466

Heelis, R. A., Lowell, J. K., & Spiro, R. W. (1982). A model of the high-latitude ionospheric convection pattern. *Journal of Geophysical Research*, *87*(A8), 6339–6345. https://doi.org/10.1029/JA087iA08p06339

Immel, T. J., Crowley, G., Craven, J. D., & Roble, R. G. (2001). Dayside enhancements of thermospheric O/N_2 following magnetic storm onset. *Journal of Geophysical Research*, *106*(A8), 15471–15488. https://doi.org/10.1029/2000ja000096

Immel, T. J., Forbes, J. M., Nerem, R. S., Sutton, E. K., & Crowley, G. (2008). Neutral composition and density effects in the October–November 2003 magnetic storms this storm, this volume.

Kil, H., Kwak, Y.-S., Paxton, L. J., Meier, R. R., & Zhang, Y. (2011a). O and N_2 disturbances in the F region during the 20 November 2003 storm seen from TIMED/GUVI. *Journal of Geophysical Research*, *116*(A2), A02314. https://doi.org/10.1029/2010JA016227

Kil, H., Lee, W. K., Shim, J., Paxton, L. J., & Zhang, Y. (2013). The effect of the 135.6 nm emission originated from the ionosphere on the TIMED/GUVI O/N_2 ratio. *Journal of Geophysical Research: Space Physics*, *118*(2), 859–865. https://doi.org/10.1029/2012JA018112

Kil, H., Paxton, L. J., Kim, K.-H., Park, S., Zhang, Y., & Oh, S.-J. (2011b). Temporal and spatial components in the storm-time ionospheric disturbances. *Journal of Geophysical Research*, *116*(A11), A11315. https://doi.org/10.1029/2011JA016750

Lee, W. K., Kil, H., Paxton, L. J., Zhang, Y., & Shim, J. S. (2013). The effect of geomagnetic-storm-induced enhancements to ionospheric emissions on the interpretation of the TIMED/GUVI O/N_2 ratio. *Journal of Geophysical Research: Space Physics*, *118*(12), 7834–7840. https://doi.org/10.1002/2013JA019132

Lei, J., Thayer, J. P., Burns, A. G., Lu, G., & Deng, Y. (2010). Wind and temperature effects on thermosphere mass density response to the November 2004 geomagnetic storm. *Journal of Geophysical Research*, *115*(A5), A05303. https://doi.org/10.1029/2009JA014754

Liou, K., Newell, P. T., Anderson, B. J., Zanetti, L., & Meng, C.-I. (2005). Neutral composition effects on ionospheric storms at middle and low latitudes. *Journal of Geophysical Research*, *110*(A5), A05309. https://doi.org/10.1029/2004JA010840

Meier, R. R. (2021). The thermospheric column O/N_2 ratio. *Journal of Geophysical Research: Space Physics*, *126*(3), e2020JA029059. https://doi.org/10.1029/2020JA029059

Meier, R. R., Picone, J. M., Drob, D., Bishop, J., Emmert, J. T., Lean, J. L., et al. (2015). Remote sensing of Earth's limb by TIMED/GUVI: Retrieval of thermospheric composition and temperature. *Earth and Space Science*, *2*, 1–37. https://doi.org/10.1002/2014EA000035

Richmond, A. D., Ridley, E. C., & Roble, R. G. (1992). A thermosphere/ionosphere general circulation model with coupled electrodynamics. *Geophysical Research Letters*, *19*(6), 601–604. https://doi.org/10.1029/92gl00401

Rishbeth, H. (1998). How the thermospheric circulation affects the ionosphere. *Journal of Atmospheric and Solar-Terrestrial Physics*, *60*(14), 1385–1402. https://doi.org/10.1016/S1364-6826(98)00062-5

Roble, R. G., & Ridley, E. C. (1987). An auroral model for the NCAR thermosphere general circulation model (TGCM). *Annales Geophysicae*, *5*(6), 369–382.

Roble, R. G., Ridley, E. C., Richmond, A. D., & Dickinson, R. E. (1988). A coupled thermosphere/ionosphere general circulation model. *Geophysical Research Letters*, *15*(12), 1325–1328. https://doi.org/10.1029/gl015i012p01325

Solomon, S. C., & Qian, L. (2005). Solar extreme-ultraviolet irradiance for general circulation models. *Journal of Geophysical Research*, *110*(A10), A10306. https://doi.org/10.1029/2005JA011160

Strickland, D. J., Bishop, J., Evans, J. S., Majeed, T., Shen, P. M., Cox, R. J., et al. (1999). Atmospheric ultraviolet radiance integrated code (AURIC): Theory, software architecture, inputs, and selected results. *Journal of Quantitative Spectroscopy & Radiative Transfer*, *62*(6), 689–742. https://doi.org/10.1016/s0022-4073(98)00098-3

Strickland, D. J., Daniell, R. E., & Craven, J. D. (2001). Negative ionospheric storm coincident with DE-1 observed thermospheric disturbance on October 14, 1981. *Journal of Geophysical Research*, *106*(A10), 21049–21062. https://doi.org/10.1029/2000ja000209

Strickland, D. J., Evans, J. S., & Paxton, L. J. (1995). Satellite remote sensing of thermospheric O/N_2 and solar EUV. 1. Theory. *Journal of Geophysical Research*, *100*(A7), 12217–12226. https://doi.org/10.1029/95ja00574

Wang, Z., Zou, S., Liu, L., Ren, J., & Aa, E. (2021). Hemispheric asymmetries in the mid-latitude ionosphere during the September 7–8, 2017 storm: Multi-instrument observations. *Journal of Geophysical Research: Space Physics*, *126*(4), e2020JA028829. https://doi.org/10.1029/2020ja028829

Yu, T. (2022). Vertical variations in thermospheric O/N_2 and the relationship between O and N_2 perturbations during a geomagnetic storm [Dataset]. Zenodo. https://doi.org/10.5281/ZENODO.7479451

Yu, T., Cai, X., Ren, Z., Li, S., Pedatella, N., & He, M. (2022a). Investigation of the $\Sigma O/N_2$ depletion with latitudinally tilted equatorward boundary observed by GOLD during the geomagnetic storm on April 20, 2020. *Journal of Geophysical Research: Space Physics*, *127*(12), e2022JA030889. https://doi.org/10.1029/2022ja030889

Yu, T., Ren, Z., Le, H., Wan, W., Wang, W., Cai, X., & Li, X. (2020). Seasonal variation of O/N_2 on different pressure levels from GUVI limb measurements. *Journal of Geophysical Research: Space Physics*, *125*(8), e2020JA027844. https://doi.org/10.1029/2020JA027844

Yu, T., Wang, W., Ren, Z., Cai, X., Liu, L., He, M., et al. (2022b). Diagnostic analysis of the physical processes underlying the long-duration $\Sigma O/N_2$ depletion during the recovery phase of the 8 June 2019 geomagnetic storm. *Journal of Geophysical Research: Space Physics*, *127*(12), e2022JA031075. https://doi.org/10.1029/2022ja031075

Yu, T., Wang, W., Ren, Z., Cai, X., Yue, X., & He, M. (2021b). The response of middle thermosphere (~160 km) composition to the November 20 and 21, 2003 superstorm. *Journal of Geophysical Research: Space Physics*, *126*(10), e2021JA029449. https://doi.org/10.1029/2021JA029449

Yu, T., Wang, W., Ren, Z., Yue, J., Yue, X., & He, M. (2021a). Middle-low latitude neutral composition and temperature responses to the 20 and 21 November 2003 superstorm from GUVI dayside limb measurements. *Journal of Geophysical Research: Space Physics*, *126*(8), e2020JA028427. https://doi.org/10.1029/2020JA028427

Yue, J., Jian, Y., Wang, W., Meier, R. R., Burns, A., Qian, L., et al. (2019). Annual and semiannual oscillations of thermospheric composition in TIMED/GUVI limb measurements. *Journal of Geophysical Research: Space Physics*, *124*(4), 3067–3082. https://doi.org/10.1029/2019JA026544

Zhai, C., Cai, X., Wang, W., Coster, A., Qian, L., Solomon, S. C., et al. (2023). Mid-latitude ionospheric response to a weak geomagnetic activity event during solar minimum. *Journal of Geophysical Research: Space Physics*, *128*(1), e2022JA030908. https://doi.org/10.1029/2022JA030908

Zhang, Y., Paxton, L. J., Morrison, D., Wolven, B., Kil, H., Meng, C.-I., et al. (2004). O/N_2 changes during 1–4 October 2002 storms: IMAGE SI-13 and TIMED/GUVI observations. *Journal of Geophysical Research*, *109*(A10), A10308. https://doi.org/10.1029/2004JA010441